Synthesis, characterization and photovoltaic properties of three new 3,4-dithienyl-substituted polythiophene derivatives

Shaojie Chen, Zhiyang Liu and Ziyi Ge

Three 3,4-dithienyl-substituted polythiophene derivatives have been synthesized and characterized. Polymer P2 exhibits the widest light absorption spectrum of the polymers in its polymer chain, which has an alternative donor-acceptor structure. Copolymers blended with 6,6-phenyl-C71-butyric acid methyl ester($PC_{71}BM$) as active layers are used to fabricate polymer solar cells (PSCs), and a variety of post-treatments are employed to optimize the PSCs performance. A maximum power conversion efficiency (PCE) of 1.22% is achieved for the conventional configuration device based on P2, and the inverted configuration device of P2 is also prepared for comparison. The results show that the inverted P2 device exhibits a better PCE (1.47%) than that of the conventional device due to the TiO_2 nanoparticles and the close energy alignment between the work function of the MoO_3 and the HOMO energy levels, which facilitate a light absorption increase and improved charge transport.

INTRODUCTION

Polymer solar cells (PSCs) have received significant attention because of their many unique merits, such as easy fabrication, low cost, light weight and flexibility.[1–7] Over the past decade, many promising materials have been synthesized; however, most of these materials are very costly and difficult to prepare. Polythiophenes are one of the most widely studied class of conjugated polymers because of their ease of synthesis and their desirable electrical and optical properties.[8,9] The extent of conjugation in thiophene-based materials depends largely on the nature of the substituents at the 3- and 4-positions. However, the studies concerning the substituents in thiophene-based materials predominantly focus on alkyl substituents at the 3-position, such as poly(3-alkylthiophene) and its derivatives.[10] A major drawback of most polythiophenes for their application in PSCs is the rather poor match between their absorption spectrum and the solar spectrum. The maximum absorbance wavelength for most poly(3-alkylthiophene) derivatives is below 700 nm ($E_g = 1.9 \sim 2.1$ eV),[11–13] which is on the far blue end of the spectrum. Several approaches have been described in the literature to tune the band gap of polythiophenes.[14,15] For instance, Andersson discussed the possibility of a polythiophene where all the molecules are added in a head to tail manner, or can be random with the occasional head to tail, head to head or tail to tail coupling as shown in Scheme 1. In addition, various types of synthetic strategies, such as Yamamoto, Lin and Dudek coupling reactions that lead to polythiophenes, have been compared by many research groups. However, the concept of using thienyl-based solubilizing groups on the thiophene main chain to extend the conjugation has not been explored widely.

Josemon Jacob[16] synthesized and characterized 3,4-diaryl-substituted polythiophene derivatives for the first time in 2011. They identified a new class of thiophene-based materials with improved conjugation and charge transport. 4-octylphenyl substituents and 5-octyl-2-thienyl substituents were used at the 3- and 4-positions of thiophene instead of simple alkyl substituents; they found that the aryl substituent on the side chain is conjugated with the main chain, leading to a lower band gap in such materials, which is good for sunlight absorption. Unfortunately, the photovoltaic properties were not investigated. In this paper, three new 3,4-dithienyl-substituted polythiophene derivatives are reported, and their photovoltaic properties are investigated systematically. In the literature,[17,18] it has been reported that 3,4-dialkyl-substituted polythiophenes suffer from severe steric hindrance between side chains and thiophene rings. To reduce these steric interactions in these three polymers, a 3,4-di(5'-isooctyl-2'-thienyl)thiophene unit (I3T) is polymerized with 5,5'-bis(tributylstannyl)-2,2'-dithienyl, 4,7-bis(5-(tributylstannyl))thiophen-2-yl)benzo[c][1,2,5]thiadiazole and 2,5-bis(tributylstannyl)thieno[3,2–b]thiophene, respectively, by a Stille coupling reaction. Their molecular structures are shown in Scheme 2.

EXPERIMENTAL PROCEDURE

General instrumentations

^{1}H nuclear magnetic resonance (NMR) spectra were recorded with a Bruker DMX-400 spectrometer (Rheinstetten, Germany). Thermogravimetric analysis

Ningbo Institute of Materials Technology & Engineering, Chinese Academy of Sciences, Ningbo, China
Correspondence: Professor Z Ge, Ningbo Institute of Materials Technology & Engineering, Chinese Academy of Sciences, zhongguan west road 1219#, Ningbo, Zhejiang 315201, China.
E-mail: geziyi@nimte.ac.cn

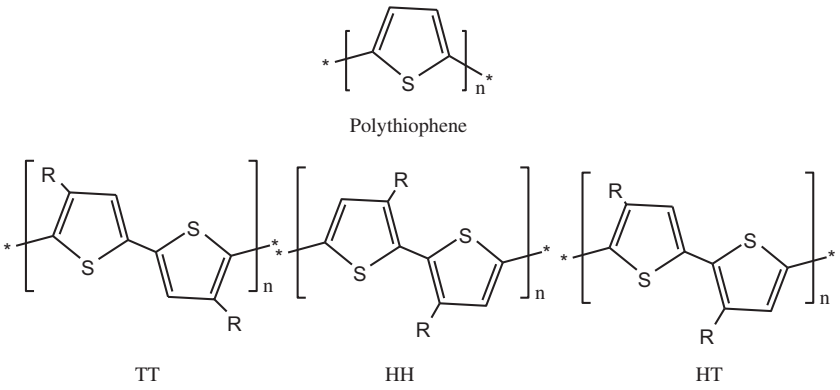

Scheme 1 Structure of polythiophene and substituted derivatives of polythiophene in HH, HT and TT couplings. HH, head to head; HT, head to tail; TT, tail to tail.

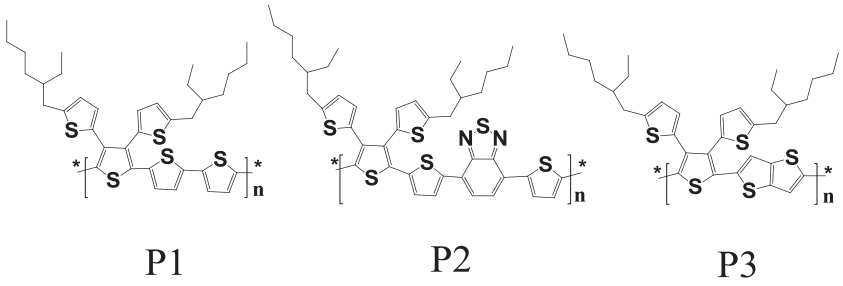

Scheme 2 Molecular structures of polymers P1, P2 and P3.

was performed using a PerkinElmer Pyris (Waltham, MA, USA). The molecular weights of the polymers were measured by the Gel Permeation Chromatography (GPC) method on a Waters 1515 (Milford, MA, USA) instrument calibrated with polystyrene standards at room temperature using chloroform as the eluent. Ultraviolet–visible (UV–vis) absorption spectra were recorded on a PerkinElmer Lambda 950. The cyclic voltammetry (CV) of the copolymer films was studied on a CHI650B potentiostat (Tennison Hill Drive, Austin, TX, USA). The surface images were obtained on a Veeco Dimension 3100 V atomic force microscope (Rheinstetten, Germany). The current-voltage (I–V) characteristics of all photovoltaic cells were measured under simulated solar light (100 mW cm^{-2}; AM 1.5 G) provided by a Newport-Oriel Sol3A 450 W solar simulator (Irvine, CA, USA) and stored under an Ar atmosphere without encapsulation. The electrical data were recorded on a Keithley 2400 source-measure unit. The intensity of the simulated solar light was calibrated using a standard Si photodiode detector (PV measurements), which was calibrated at the National Renewable Energy Laboratory in the United States.

Materials

All chemicals and solvents used were reagent grade and purchased from Aldrich (St Louis, MO, USA), TCI (Tokyo, Japan) or Acros Organics Company (Brussels, Belgium). The solvents used in the reactions and photophysical measurements were all distilled after dehydration according to conventional methods.

PSC device fabrication and characterization

The PSCs were fabricated on the basis of a conventional configuration (ITO/PEDOT:PSS/PX(x = 1,2,3):$PC_{71}BM$/Ca/Al) and an inverted configuration (FTO/TiO_2/PX(x = 1,2,3):$PC_{71}BM$/MoO_3/Ag). The ITO/FTO electrodes ($\leqslant$14 Ω per square) were cleaned by a routine cleaning procedure that includes manual washing in aqueous detergent, and then sequential sonication in acetone, isopropanol and deionized water. They were then rinsed with ethanol and dried under a N_2 stream before being modified with a 40-nm thick spin-cast layer of PEDOT/PSS 'Clevios PVP AI 4083' (HC Stark, Frankfurt, Germany), which was dried at 120 °C for 20 min. The Clevios suspension was stirred and filtered through a 0.45 μm syringe filter prior to casting. FTO substrates were cleaned using the same method as the ITO electrodes. A TiO_2 layer was prepared through the following steps:[19] tetrabutyl titanate (Ti$(OC_4H_9)_4$), acetylacetone and ethanol were mixed in the volume ratio of 1:0.5:6, and the mixture was stirred at room temperature until a homogeneous yellow stable TiO_2-sol was obtained. Then, the solution was spin coated on an FTO glass at 4000 r.p.m. for 60 s, followed by sintering at 450 °C for 1 h under ambient conditions. An active layer was spin coated on top of the PEDOT/PSS or TiO_2 layer at 1000 r.p.m. In a conventional configuration, a 20-nm thick calcium (Ca) layer and 100-nm thick aluminum (Al) layer were thermally evaporated at a pressure of ~ 10^{-6} mbar. In the inverted configuration, a 20-nm thick MoO_3 layer and a 100-nm thick Ag layer were deposited. The mask geometry defined an effective device area of 0.1257 cm^2. The sketch map of the traditional constructure cell and inverted constructure cell are shown in Figure 1.

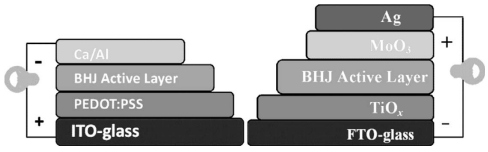

Figure 1 A sketch map of a traditional constructure cell (left) and an inverted constructure cell (right). A full color version of this figure is available at *Polymer Journal* online.

Synthesis of 3,4-di-(5'-isooctyl-2'-thienyl)-2,5-dibromothiophene

The synthetic route to 3,4-di-(5'-isooctyl-2'-thienyl)-2,5-dibromothiophene is shown in Figure 2. ^1H NMR spectra of all the monomers (a–e) are shown in Figures 3,4,5 and 6, respectively.

Synthesis of 2-isooctyl-thiophene (a). N-butyl lithium (2.5 M in hexane; 60 ml, 0.15 mol) was added dropwise to a solution of thiophene (15 g, 0.18 mol) in 150 ml of tetrahydrofuran (THF) at −78 °C. After 45 min, 27 g of 1-bromo-2-ethylhexane (0.14 mol) was added to the above solution. The reaction mixture was stirred for another 3 h at room temperature and then poured into water. The mixture was extracted with ether, dried over magnesium sulfate and then the solvent was evaporated. The compound was purified by vacuum distillation. 24.2 g of pure product (colorless liquid) was obtained (yield: 96%). ^{1}H NMR (400 MHz, $CDCl_3$) δ 7.23 (s, 1H, J=8.51 Hz), 7.19 (s, 1H, J=8.19 Hz), 7.13 (s, 1H), 2.78 (d, 2H, J=7.53 Hz), 1.86 (s, 1H), 0.89–1.55 (m, 15H; Figure 3). Elemental analysis: calculated (calcd) for $C_{12}H_{20}S$, 196, C, 73.47%; H, 10.2%; found: C, 74.20%; H, 11.31%.

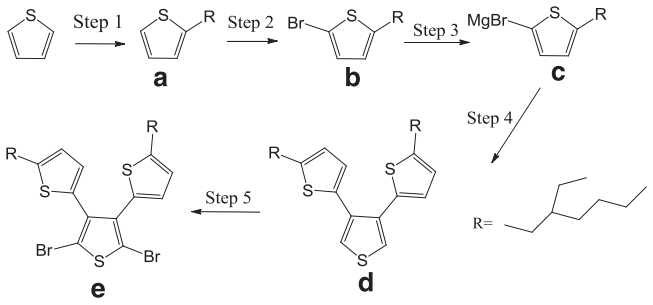

Figure 2 The synthetic route for the synthesis of 3,4-di-(5′-isooctyl-2′-thienyl)-2,5-dibromothiophene (**a**–**e**, respectively means the intermediate compound of each step).

Synthesis of 2-bromo-5-isooctyl-thiophene (b). For the synthesis of 2-bromo-5-isooctyl-thiophene, 25.6 g of N-bromobutanimide (NBS) in 50 ml of N,N-Dimethylformamide (DMF) was added dropwise under darkness to a solution containing 24 g of **a** in DMF at 0 °C. The reaction mixture was stirred at room temperature for another 10 h and then poured into water. After extraction with methylene chloride, the organic phase was separated and dried over magnesium sulfate. The final pure product (colorless liquid) was obtained through vacuum distillation. (28 g, yield: 80%). ^{1}H NMR (400 MHz, $CDCl_3$) δ 7.19 (s, 1H, J=8.19 Hz), 7.13 (s, 1H), 2.78 (d, 2H, J=7.53 Hz), 1.86 (s, 1H), 0.89–1.55

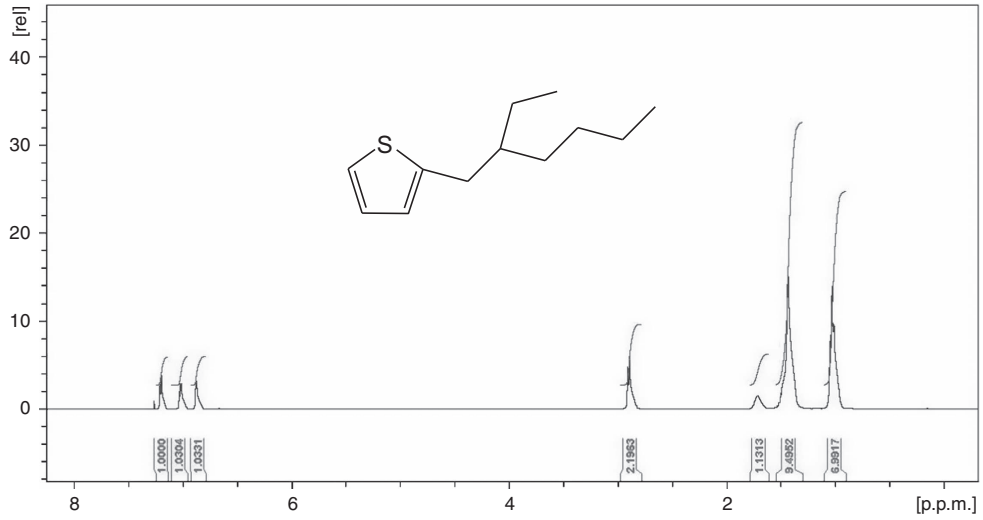

Figure 3 ^{1}H nuclear magnetic resonance spectrum of 2-isooctyl-thiophene. A full color version of this figure is available at *Polymer Journal* online.

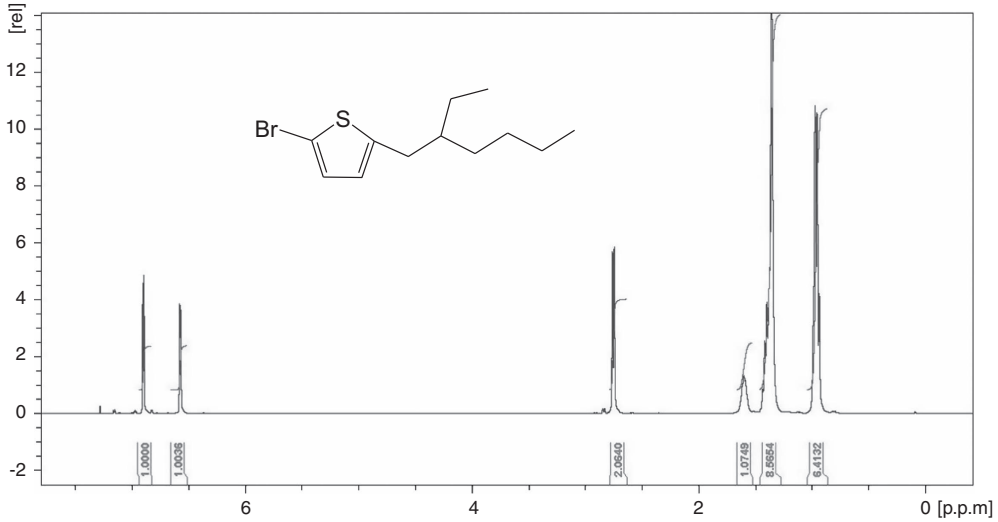

Figure 4 ^{1}H nuclear magnetic resonance spectrum of 2-bromo-5-isooctyl-thiophene. A full color version of this figure is available at *Polymer Journal* online.

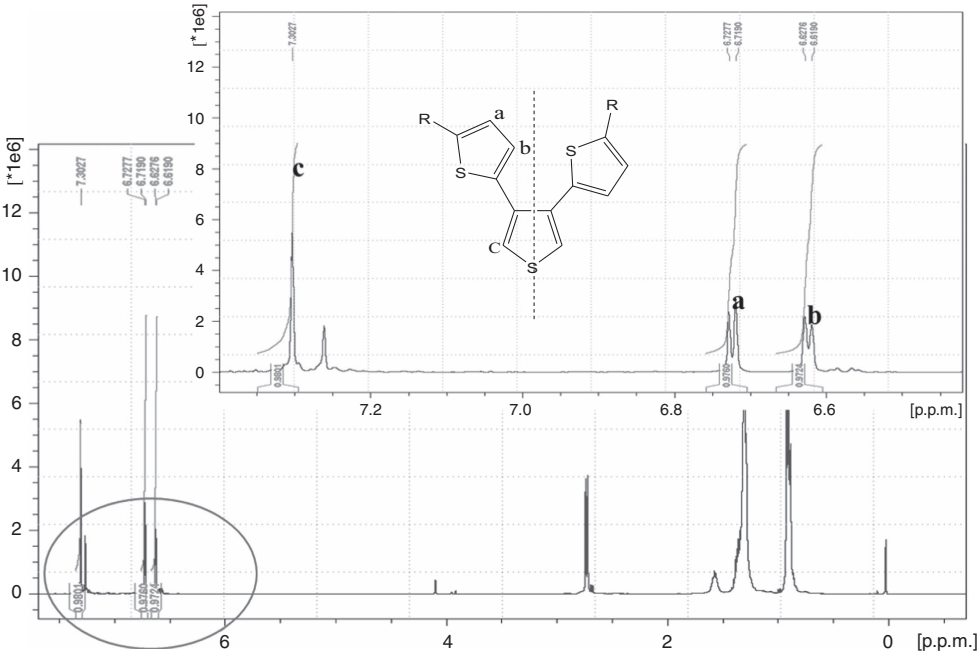

Figure 5 ^{1}H nuclear magnetic resonance spectrum of 3,4-di-(5'-isooctyl-2'-thienyl)thiophene. A full color version of this figure is available at *Polymer Journal* online.

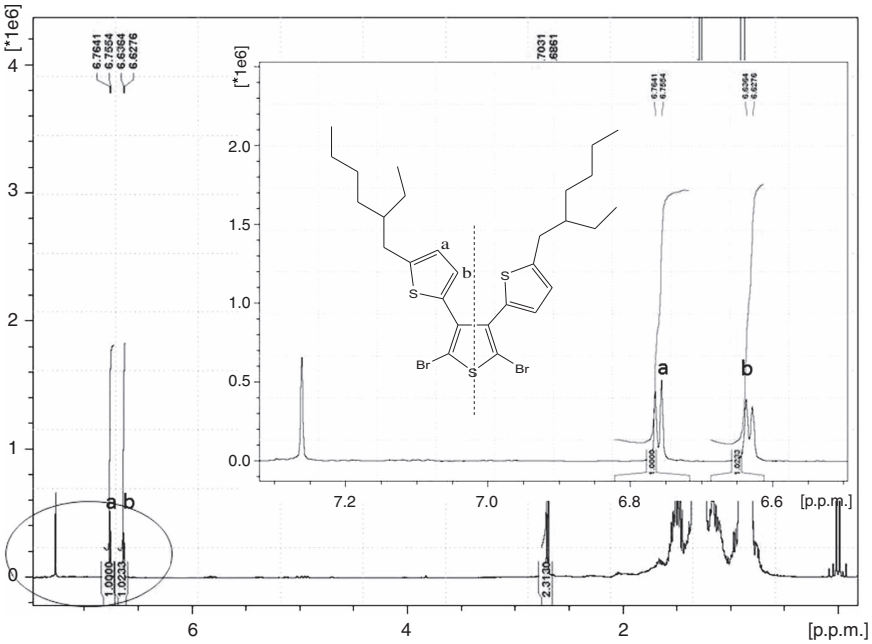

Figure 6 ^{1}H nuclear magnetic resonance spectrum of 3,4-di-(5'-isooctyl-2'-thienyl)-2,5-dibromothiophene. A full color version of this figure is available at *Polymer Journal* online.

(m, 16H; Figure 4). Elemental analysis: calcd for $C_{12}H_{19}SBr$, 275, C, 52.36%; H, 6.91%; found: C, 54.23%; H, 7.11%.

Synthesis of 3,4-di-(5'-isooctyl-2'-thienyl)thiophene (d). Magnesium turnings (0.416 g, 17.34 mmol) and a catalytic amount of iodine were added to a solution of **b** (4.77 g, 17.34 mmol) in dry tetrahydrofuran (15 ml). The resulting mixture was stirred at 65 °C for 3 h to obtain **c**. The Grignard reagent was slowly transferred to a solution of 3,4-dibromothiophene (0.932 g, 3.85 mmol) and Ni(dppp)Cl_2 (2 mol%, 42 mg) in dry tetrahydrofuran (10 ml). After stirring for 20 h at 75 °C, the reaction was quenched with 2 N HCl. Then, the reaction mixture was extracted with $CHCl_3$, and the extract was washed with brine and dried over Na_2SO_4. The residue was purified using column chromatography with pure hexane as eluent to yield the target compound as a light yellow liquid. (1.08 g, yield: 60%) ^{1}H NMR (400 MHz, $CDCl_3$) δ 7.23

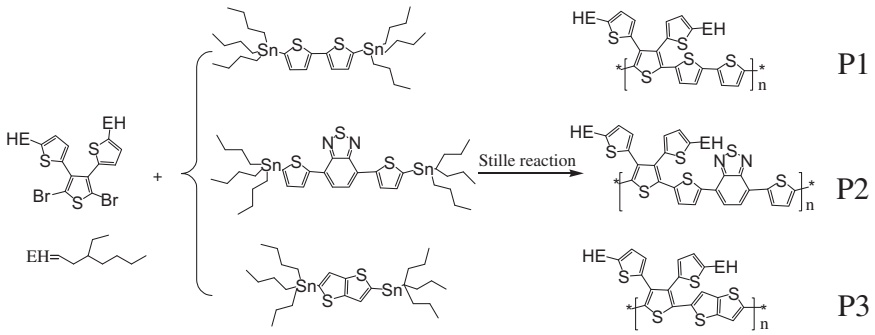

Figure 7 The synthetic route for the synthesis of polymers P1–P3.

(s, 2H, $J = 8.51$ Hz), 6.75 (d, 2H, $J = 8.19$ Hz), 6.68 (s, 2H), 2.78 (d, 4H, $J = 7.53$ Hz), 1.86(s, 2H), 0.89–1.55 (m, 30H; Figure 5). Elemental analysis: calcd for $C_{28}H_{40}S_3$, 472, C, 71.19%; H, 8.47%; found: C, 74.32%; H, 9.11%.

Synthesis of I3T (e). NBS (0.462 g, 2.25 mmol) was added to a solution of **d** (0.52 g, 1.11 mmol) in $CHCl_3$ (15 ml), and the resulting mixture was stirred at 0 °C for 30 min. The reaction mixture was poured into water, extracted with $CHCl_3$ and then dried over Na_2SO_4. After the evaporation of the solvent, the crude product was purified using column chromatography with pure hexane as eluent to yield the target compound as a yellow liquid. (0.55 g, yield: 90%) ^{1}H NMR (400 MHz, $CDCl_3$) δ 6.75 (s, 2H, $J = 8.19$ Hz), 6.68 (s, 2H), 2.78 (d, 4H, $J = 7.53$ Hz), 1.86(s, 2H), 0.89–1.55 (m, 30H; Figure 6). Elemental analysis: calcd for $C_{28}H_{38}S_3Br_2$, 630, C, 53.33%; H, 6.03%; found: C, 54.33%; H, 7.52%.

Synthesis of I3T-based polymers

Three polymers were prepared using the same procedure as coupling dibromide compounds with bis(tributylstannyl)-substituted compounds via the Stille coupling reaction. 5,5'-bis(tributylstannyl)-2,2'-dithienyl, 4,7-bis(5-(tributylstannyl))thiophen-2-yl)benzo[c][1,2,5]thiadiazole and 2,5-bis(tributylstannyl) thieno[3,2–b]thiophene were obtained from the Derthon Optoelectronic Materials Science and Technology (Shengzhen, China). Figure 7 shows the synthetic routes of the polymers P1–P3.

One millimole of the dibromide compound, 1.0 mmol of the bis(tributylstannyl)-substituted compound and 50 ml of toluene were placed into a three-necked flask that was then placed into an oil bath. The solution was flushed with nitrogen for 10 min, and then 20 mg of $Pd(PPh_3)_4$ was added to the flask. The solution was flushed again for 20 min. The reaction mixture was stirred at 120 °C for 20 h under a nitrogen atmosphere. Then, the mixture was cooled to room temperature, and the polymer was precipitated by the addition of 100 ml of methanol and filtered through a soxhlet thimble. The filtered polymer was subjected to soxhlet extraction with methanol, hexane and chloroform, successively, and then recovered as a solid sample from the chloroform fraction by rotary evaporation. The solid was dried under vacuum for 1 day to obtain the final product. The polymerization reaction yield was ~40–60%.

Poly[3,4-di-(5'-isooctyl-2'-thienyl)-2,5-thiophene-(2,2'-dithienyl)] (P1). ^{1}H NMR ($CDCl_3$, p.p.m.): δ 0.89 (m, -CH_3), 1.25–1.96 (m, -CH_2-), 1.88 (s, $(CH_2)_3CH$), 6.63–7.40 (d, thienyl-H). Elemental analysis: calcd for $(S_5C_{36}H_{42})_n$, $(634)_n$ calcd: C, 68.14%; H, 6.62%; found: C, 65.6%; H, 6.33%. GPC: $M_w = 63.3$ K, $M_n = 35.2$ K, PDI = 1.80.

Poly{3,4-di-(5'-isooctyl-2'-thienyl)-2,5-thiophene-[4,7-(2-dithienyl)-2,1,3-benzothiadiazole]} (P2). ^{1}H NMR ($CDCl_3$, p.p.m.): δ 0.89 (m, -CH_3), 1.25–1.94 (m, -CH_2-), 1.88 (s, $(CH_2)_3CH$), 6.83–7.73 (d, phenyl-H), 7.80 (d, 2H, aromatic-H). Elemental analysis: calcd for $(S_6C_{42}H_{44}N_2)_n$, $(768)_n$ calcd: C, 65.63%; N, 3.65%; H, 5.73%; found: C, 63.63%; N, 4.15%; H, 4.73%. GPC: $M_w = 83.4$ K, $M_n = 41.7$ K, PDI = 2.00.

Poly[3,4-di-(5'-isooctyl-2'-thienyl)-2,5-thiophene-(thieno[3,2–b]thiophene)] (P3). ^{1}H NMR ($CDCl_3$, p.p.m.): δ 0.89 (m, -CH_3), 1.25–1.96 (m, -CH_2-), 1.88 (s, $(CH_2)_3CH$), 6.83–7.73 (m, thienyl-H). Elemental analysis: calcd for $(S_5C_{34}H_{40})_n$, $(608)_n$ calcd: C, 67.11%; H, 6.58%; found: C, 65.11%; H, 5.98%. GPC: $M_w = 121.5$ K, $M_n = 49.2$ K, PDI = 2.47.

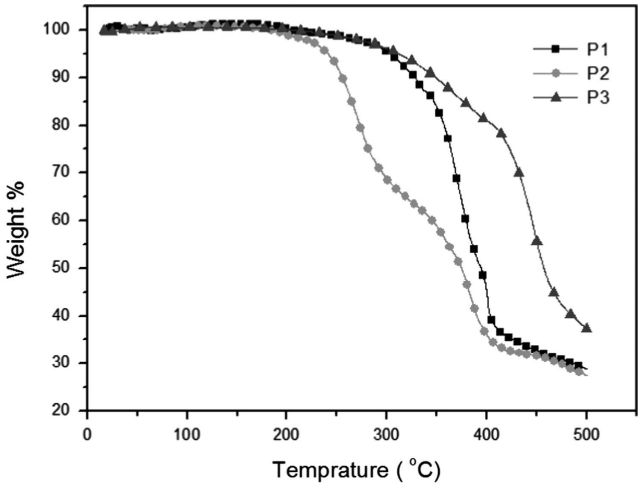

Figure 8 Thermogravimetric analysis (TGA) curves of the polymers. A full color version of this figure is available at *Polymer Journal* online.

RESULTS AND DISCUSSION

Thermostability

As revealed by the thermogravimetric analysis curves (Figure 8), thermogravimetric analysis of the polymers exhibited an apparent degradation at 304, 241 and 312 °C for P1, P2 and P3, respectively, with a weight loss of ~5% under nitrogen protection. These 3,4-dithienyl-substituted thiophene-based polymers showed relatively poor thermal stability compared with the reported materials (282–448 °C).[16] This is likely due to the introduction of ethylene groups along the backbone of the reported materials resulting in better rigid coplanarity, leading to a higher thermal decomposition temperature than that of the synthesized polymers. Nevertheless, the thermal stability of the three polymers investigated is adequate for their application in PSCs and other optoelectronic devices in the general environment.

Optical properties

Figure 9 shows the normalized absorption spectra of these three polymers in a $CHCl_3$ solution and their corresponding spin-coated films on quartz substrates. The results from the absorption spectra are summarized in Table 1. Among them, the UV–vis spectrum in P2 films exhibit the lowest energy absorption edge at a longer wavelength

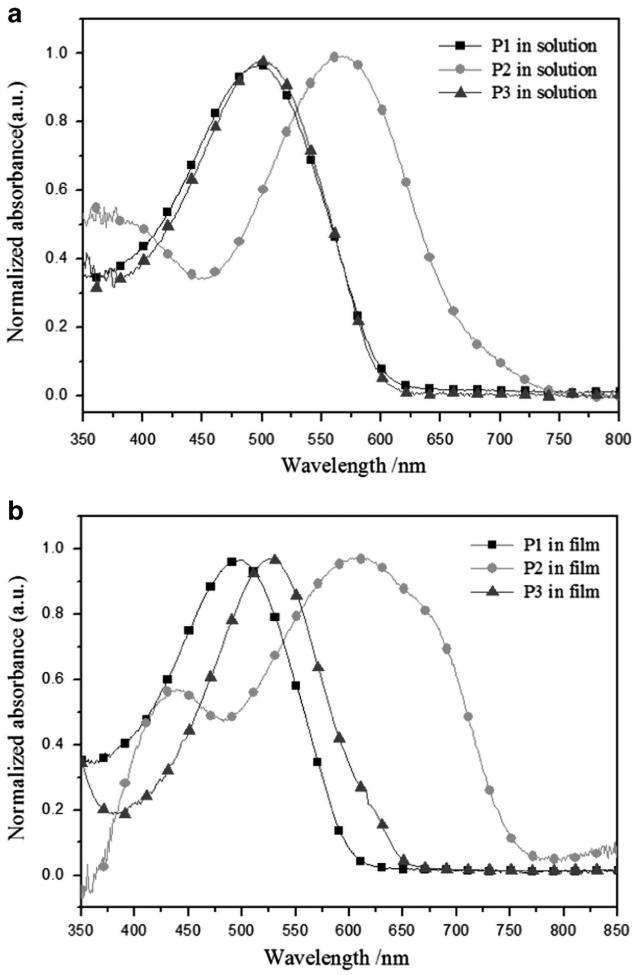

Figure 9 Ultraviolet–visible absorption spectra of polymers P1–P3 in a $CHCl_3$ solution (**a**) and as thin films (**b**). A full color version of this figure is available at *Polymer Journal* online.

Table 1 Optical data for P1–P3 in dilute $CHCl_3$ solutions and in the solid films

Polymer	λ_{max} *(nm)*		[a]λ_{onset} *(nm)*		[b]E^{opt} *(eV)*
	Solution	*Film*	*Solution*	*Film*	
P1	495	498	604	606	2.05
P2	570	612	727	765	1.62
P3	500	526	610	653	1.89

[a]Estimated from the intersection of the fitting a tangent on the low energetic edge of the absorption spectrum with the abscissa.
[b]Calculated from the absorption edge of the polymer films, $E_g^{opt} = 1240/\lambda_{edge}$.

than that of P1 and P3, and the λ_{edge} of P2 is 765 nm. The low energy absorption edge is attributed to P2 with its alternated donor and acceptor in the main chain, which could induce an intermolecular charge transfer along the conjugated chain. This is good for UV–vis absorption, whereas P1 and P3 do not have such structures. The UV–vis spectra of P3 show a $\lambda_{edge} =$ 653 nm in the film, a little longer than that of P1 ($\lambda_{edge} =$ 606 nm). The thieno[3,2–b]thiophene unit in P3 has a better coplanarity than the 2,2'-dithienyl unit in P1 as shown in Figure 10, which presents a wider UV–vis absorption spectra than that of P1. Thus, we can conclude that incorporating the electron-acceptor unit into the polymer chain can lower the polymer band gap effectively. The geometry optimization structures of polymers ($n = 2$) by computer simulation as shown in Figure 10 indicate that P2 has the best coplanarity with a dihedral angle of 154°, and P1 and P3 have similar dihedral angles of 125° and 130°, respectively. All calculations were performed with the Gaussian 03 program (Wallingford, CT, USA). The geometries of the oligomers were optimized at a Restricted Hartree-Fock (RHF) level using a semi-empirical AM1 method. Thus, we can conclude that the greater the coplanarity, the more the polymer chain is sufficient for the reduction of the band gap. In addition, it should be noted that although 3,4-dithienyl-substituted thiophene displays a better coplanarity than that of the 3-position thiophene unit, there is a severe steric hindrance between thienyls. Figure 10 shows that the thienyls on the 3,4-position frequently twist and do not maintain a good coplanarity, which results in a reduction in the limiting band gap. The P1 and P3 band gaps are close to that of the poly(3-alkylthiophene) derivatives.

Table 1 shows that the spectra of all the polymers in the solid-state films are red-shifted compared with their corresponding absorption onset in solution. This phenomenon suggests that the polymer backbone in the solid-state has a more ordered interchain stacking compared with that in solution.[20,21] The absorption band-edge of the polymer films extend to 606, 765 and 653 nm, which red-shift by 2, 38 and 43 nm compared with those in solution, respectively. Thus, the optical band gaps (E_g^{opt}) were calculated to be 2.05, 1.62 and 1.89 eV for P1, P2 and P3, respectively.

In summary, all these polymers show absorption bands between 300–800 nm with corresponding optical band gaps from 1.62 to 2.05 eV. Obviously, the wider absorption band and the lower optical band gap of the polymer are favorable to their application in PSCs.

Electrochemical properties

Electrochemical CV was performed to determine the highest occupied molecular orbital (HOMO) and lowest unoccupied molecular orbital (LUMO) energy levels of the synthesized polymers. Figure 11 shows the CV of the I3T-based polymer films on Pt electrodes in a 0.1 mol l^{-1} Bu_4NPF_6 CH_3CN solution. From the onset oxidation potential (E_{ox}) and onset reduction potential (E_{red}) of the polymers, the HOMO and LUMO energy levels and the band gap (E_g^{ec}) were calculated and are listed in Table 2.

Figure 11 shows the CV of the polymers P1, P2 and P3. The reductions are observed with an onset potential of ~1.21 V versus the saturated calomel electrode of P1, 0.89 V of P2 and 1.17 V of P3. Similarly, oxidations are observed with an onset potential at approximately −0.77, −0.84 and −0.68 V versus saturated calomel electrode of P1, P2 and P3, respectively. The HOMO and LUMO energy levels were calculated to be −5.61 and −3.63 eV for P1, −5.29 and −3.56 eV for P2 and −5.57 and −3.72 eV for P3 via CV using the following empirical equations: HOMO = −(E_{ox}+4.40) (eV), LUMO = −(E_{red} +4.40) (eV).[22] From the equation E_g^{ec} = LUMO − HOMO, the band gap of the polymers P1–P3 were calculated to be 1.98, 1.73 and 1.85 eV, respectively. In addition, the discrepancy between the CV band gaps with the optical band gap of the polymers is likely due to the interface barrier for charge injection.[23,24]

Photovoltaic properties

Bulk heterojunction PSCs were fabricated with a general device structure of ITO/PEDOT:PSS/PX(x = 1,2,3):$PC_{71}BM$/Ca/Al. A mixed

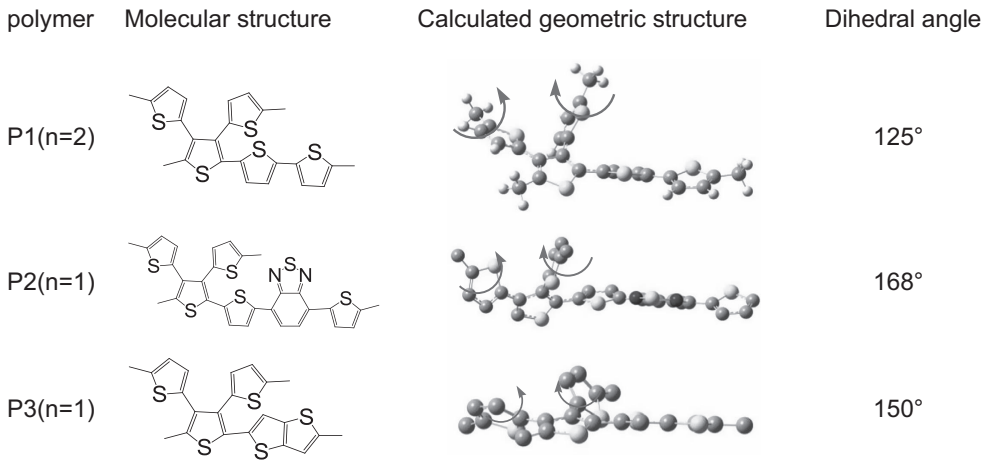

Figure 10 Geometrical optimization structures of polymers P1, P2 and P3. A full color version of this figure is available at *Polymer Journal* online.

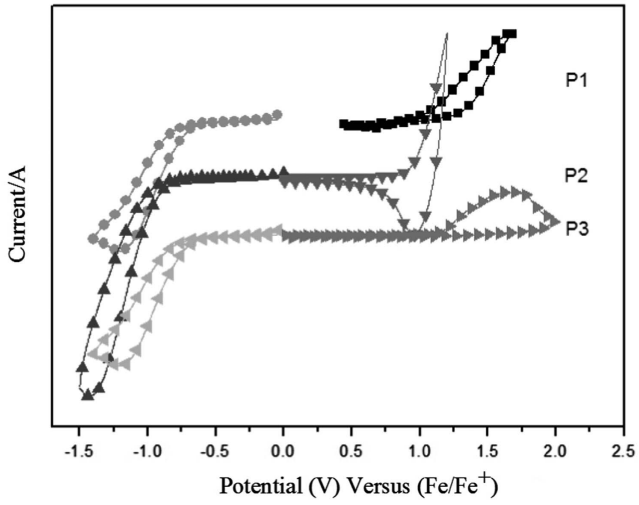

Figure 11 Cyclic voltammograms of P1–P3. A full color version of this figure is available at *Polymer Journal* online.

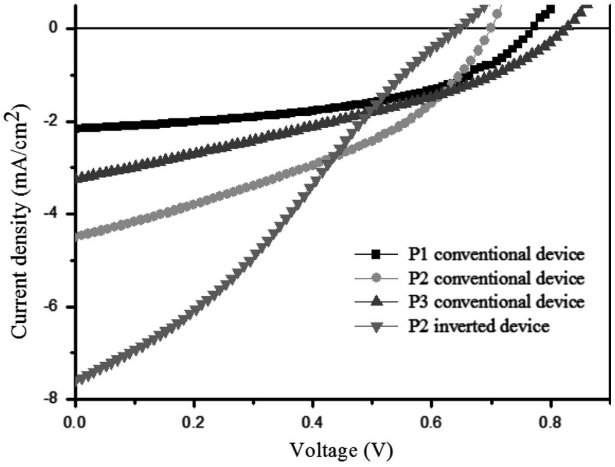

Figure 12 The J-V cures of the cells incorporating the polymers blended with $PC_{71}BM$ in a 1:3 ratio. A full color version of this figure is available at *Polymer Journal* online.

Table 2 Optical properties, electrochemical onset potentials and electronic energy levels of P1–P3

	λ_{onset} (nm)	E_g^{opt} (eV)	E_{ox} (V)	HOMO (eV)	E_{red} (V)	LUMO (ev)	E_g^{ec} (eV)
P1	606	2.05	1.21	−5.61	−0.77	−3.63	1.98
P2	765	1.62	0.89	−5.29	−0.84	−3.56	1.73
P3	653	1.89	1.17	−5.57	−0.68	−3.72	1.85

solvent of *o*-dichlorobenzene and chloroform (V/V = 1/1) was chosen to dissolve the synthesized polymer sufficiently. The photoactive layers were prepared by spin coating the blend solution of PX(x = 1,2,3): $PC_{71}BM$ dissolved in solvent. When the PEDOT:PSS was spin coated, the layer was annealed for 20 min at 140 °C, and the active layer of the polymer and $PC_{71}BM$ blends were spin coated before being annealed at 120 °C for 10 min. The Ca and Al were deposited in an evaporator at 10^{-6} Pa, and their performance was measured under 100 mW cm^{-2} AM 1.5 G illumination. The ratio of polymer to $PC_{71}BM$ examined was between 1:1 and 1:3 by weight, and the optimized conditions were 1:3 for all blends with a corresponding active layer thickness of ~ 230 nm, as detected by an ellipsometer (Angstron Sun Technologies, Boston, MA, USA). To further improve the device performance, a small amount (2 vol%) of dioxane, a high boiling point additive, was added to optimize the blend morphology. In addition, the inverted cell of FTO/TiO_2/P2:$PC_{71}BM$/MoO_3/Ag was fabricated as described in section 2.3. The current density-voltage (J-V) curves of the polymer: $PC_{71}BM$ devices are shown in Figure 12, and the photovoltaic parameters of the devices are summarized in Table 3.

As shown in Figure 12 and Table 3, the conventional devices exhibit a short-circuit current density (J_{sc}), open-circuit voltage (V_{oc}) and fill factor (FF) in the P1:$PC_{71}BM$ (1:3) solar cells of 2.17 mA cm^{-2}, 0.79 V, and 0.47, respectively, resulting in an average power conversion efficiency (PCE) of 0.81% for P1. Solar cells based on polymer P2 present a J_{sc} of 4.50 mA cm^{-2}, a V_{oc} of 0.70 V, a FF of 0.38 and a PCE of 1.22%. Solar cells based on polymer P3 show a J_{sc} of 3.26 mA cm^{-2}, a V_{oc} of 0.85 V, a FF of 0.32 and a PCE of 0.91%. As described above, solar cells based on polymer P2 exhibit the best PCE due to its

Table 3 Photovoltaic performance of polymers under the illumination of 1.5 AM with 2% DIO as additives

Polymer	*DIO (vol%)*	*J_{sc} (mA cm^{-2})*	*V_{oc} (V)*	*FF (%)*	*PCE (%)*	*Configuration*
P1	2	2.17	0.79	47.2	0.81%	Conventional
P2	2	4.50	0.70	38.7	1.22%	Conventional
P2	2	7.58	0.64	30.4	1.47%	Invert
P3	2	3.26	0.85	32.8	0.91%	Conventional

Abbreviations: DIO, dioxane; FF, fill factor; PCE, power conversion efficiency.
DIO was used as additive to improve the morphology of the films.

excellent J_{sc}. Comparison of the absorption profiles of P2 with that of P1 and P3 suggest that the enhanced current density could be, in part, due to an increased light absorption at longer wavelengths of P2 as shown in Figure 9. Comparing P3 and P1, solar cells based on P3 show a better PCE than that of P1, attributed to a better light absorption and bigger V_{oc}. In addition, we should note that solar cells based on P2 present the smallest $V_{oc,}$ ascribed to the relative higher-lying HOMO energy level of P2.

To further increase the PCE, P2 was selected to fabricate the inverted device. The inverted device configuration of FTO/TiO_2/P2:$PC_{71}BM$/MoO_3/Ag with a 1:3 (P2:$PC_{71}BM$) blend ratio was annealed at 120 °C and contained 2% DIO additives. The results show a PCE of 1.47% with a V_{oc} of 0.64 V, a J_{sc} of 7.58 mA cm^{-2}, and 30.4% of FF as shown in Figure 12 and Table 3. When compared with the conventional configuration (ITO/PEDOT:PSS/P2:$PC_{71}BM$/Ca/Al), the inverted configuration exhibited a higher PCE that can be attributed to the improved J_{sc} (7.58 mA cm^{-2} Vs 4.50 mA cm^{-2}). The improved J_{sc} might be due to the higher light absorption of the TiO_2 nanoparticles and the close energy alignment between the work function of MoO_3 and the HOMO energy levels of the polymer in the inverted configuration.

In conclusion, solar cells based on P2 exhibited the highest PCE among the three PSCs in the conventional device configuration. This property of P2 may be due to its wide absorption range, which results in the largest J_{sc} of 4.50 mA cm^{-2}. P3 displays a wider absorption range than P1, which results in a better PCE (0.91% vs 0.81%). Thus, we can conclude that the band gap of the polymer has an important role in the performance of PSCs. Both the conventional device and inverted device are configured by P2, and the results show that the PCE of the inverted solar cell device is higher than that of the conventional device. The improved efficiency of the inverted device might be due to the higher light absorption of the TiO_2 nanoparticles and the close energy alignment between the work function of the MoO_3 and the HOMO energy levels of the polymer in the inverted configuration,[25] facilitating increased light absorbance and improved charge transport.

Hole and electron mobility

The hole and electron mobilities of the active layer films based on all copolymers were investigated by the space-charge-limited current model, with a device structure of ITO/PEDOT:PSS/PX(x=1,2,3):$PC_{71}BM$/Au[26] for hole-only devices, and ITO/Al/ PX(x=1,2,3):$PC_{71}BM$/Ca/Al[27] for electron-only devices. According to the following formula modified from Mott-Gurney's Law: $J=(9/8)\varepsilon_0\varepsilon_r\mu(V^2/d^3)$, where J is the current, ε_o is the permittivity of free space (8.85×10^{-12} $CV^{-1}S^{-1}$), ε_r is the dielectric constant of the polymer with an assumed value of 3.0, μ is the charge mobility, V is the voltage drop across the device ($V=V_{appl}-V_{bi}-V_s$), and d is the active layer's thickness. The hole and electron mobilities can be calculated from the slope of the $J^{1/2}$~V curves as shown in Figure 13. The hole and electron mobilities are summarized in Table 4. The hole mobility of all copolymers was moderate given the photovoltaic donor material in PSCs.[28]

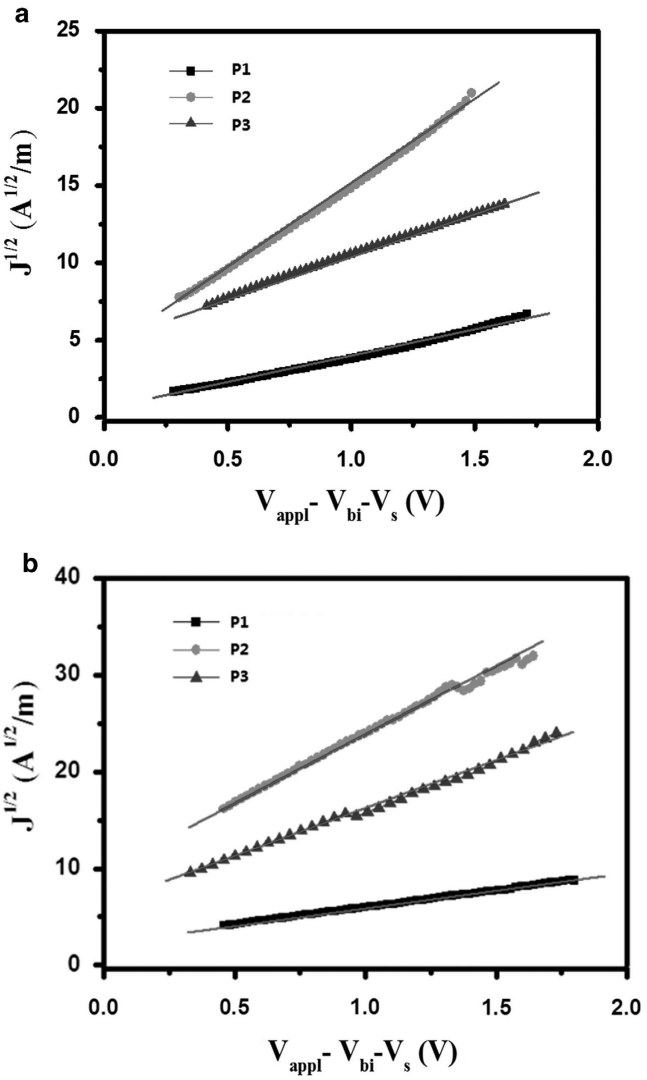

Figure 13 $J^{1/2}$~V characteristics of (**a**) the hole-only and (**b**) electron-only devices based on PX(x=1,2,3):$PC_{71}BM$ blended films. A full color version of this figure is available at *Polymer Journal* online.

Table 4 The hole and electron mobilities of P1, P2 and P3

Copolymer	*μ_h ($cm^2 V^{-1} S^{-1}$)*	*μ_e ($cm^2 V^{-1} S^{-1}$)*
P1	3.00×10^{-6}	2.90×10^{-6}
P2	4.43×10^{-5}	2.89×10^{-5}
P3	2.39×10^{-6}	7.08×10^{-6}

Morphology

The morphology of the active layer is a key requirement for achieving a high PCE.[29,30] The morphological features of the photoactive layers were investigated using tapping-mode atomic force microscopy. The atomic force microscopy topographies are shown in Figure 14. It could

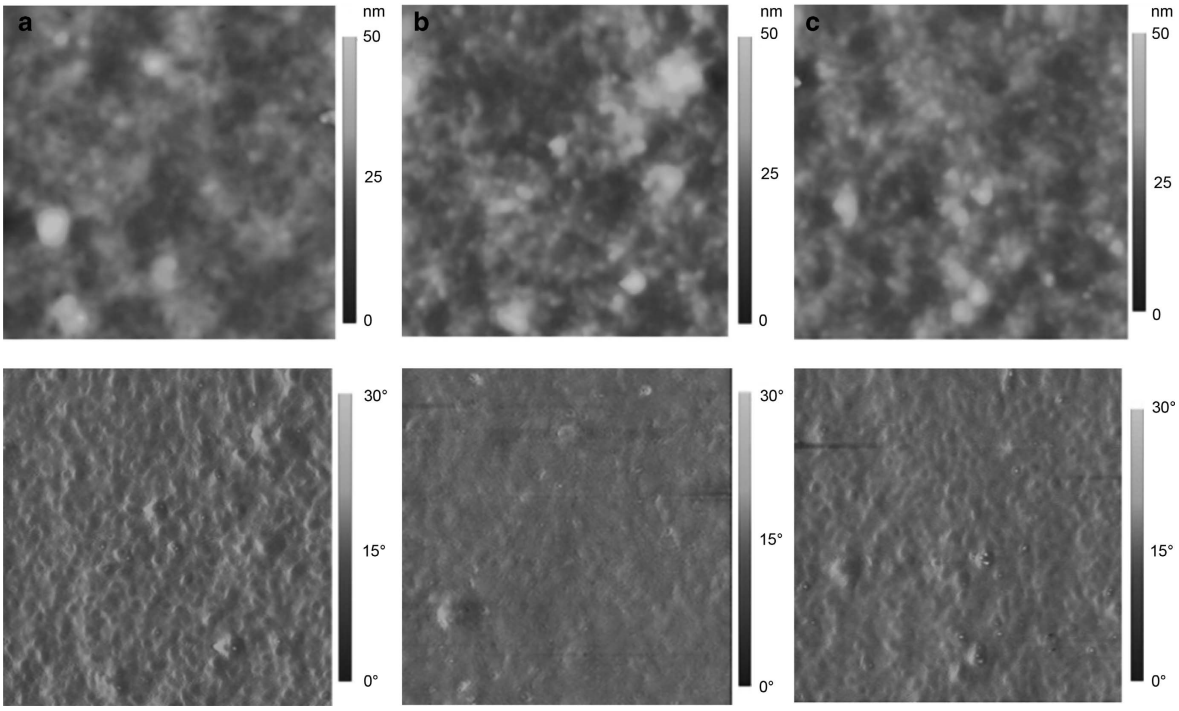

Figure 14 Tapping-mode atomic force microscopy topography images (top) and phase images (bottom) of the active layer films: (**a**) P1/$PC_{71}BM$, (**b**) P2/$PC_{71}BM$ and (**c**) P3/$PC_{71}BM$. A full color version of this figure is available at *Polymer Journal* online.

be observed that all of the PX(x = 1,2,3):$PC_{71}BM$ blends exhibit moderately homogeneous films with no large phase separation, indicating that all of them have a good miscibility with $PC_{71}BM$. All three active layers displayed no clear phase separation, and the P2:$PC_{71}BM$ blend film exhibited the highest photovoltaic performance in all copolymers-based PSCs, attributed to its superior light absorption and smooth surface.

CONCLUSION

Three new copolymers based on an I3T unit were designed and synthesized successfully in this paper. Their thermal, optical, electronic and photovoltaic properties were comprehensively characterized. Among the three copolymers, P2 exhibited the smallest band gap of 1.62 eV, which was ascribed to its polymer chain with a donor–accepter structure. Both P1 and P3 showed similar band gaps (2.05 and 1.89 eV) due to their similar molecular structures. Although the 3,4-dithienyl-substituted thiophene has a better coplanarity than the 3-position thiophene unit, severe steric hindrance between the thienyls results in a lower and limited band gap. The band gaps of P1 and P3 are similar to those of the poly(3-alkylthiophene) derivatives. Copolymers blended with $PC_{71}BM$ were used as the active layers to fabricate PSCs, and thermal annealing was employed in the presence of additives to optimize device performance. For the conventional device of ITO/PEDOT:PSS/PX(x = 1,2,3):$PC_{71}BM$/Ca/Al, P2 exhibited the best PCE of 1.22%. Comparing the conventional device with the inverted device of P2, the PCE of the inverted solar cell based on P2 was higher than that of its corresponding conventional device (1.47% vs 1.22%). The enhancement of the PCE might be due to the higher light absorption of TiO_2 nanoparticles and the close energy alignment between the work function of the MoO_3 and the HOMO energy levels of P2, facilitating increased light absorption and better charge transport. These results might supply useful information to understand the relationship between the molecular structure, device configuration and photovoltaic properties of PSCs.

CONFLICT OF INTEREST

The authors declare no conflict of interest.

ACKNOWLEDGEMENTS

The present research was financially supported by the Ningbo Natural Science Foundation (2015A610238) and China Postdoctoral Science Foundation funded project (2013M531485).

1 Wang, Y., Yang, F., Liu, Y., Peng, R., Chen, S. & Ge, Z. New alkylfuranyl-substituted benzo[1,2-b:4,5-b']dithiophene-based donor-acceptor polymers for highly efficient solar cells. *Macromolecules* **46**, 461368–461375 (2013)
2 Wang, Y., Liu, Y., Chen, S., Peng, R. & Ge, Z. Significant enhancement of polymer solar cell performance via side-chain engineering and simple solvent treatment. *Chem. Mater.* **25**, 3196–3204 (2013).
3 Zhao, W., Cai, W., Xu, R., Yang, W., Gong, X. & Wu, H. Novel conjugated alternating copolymer based on 2,7-carbazole and 2,1,3-benzoselenadiazole. *Polymer* **51**, 3196–3202 (2010).
4 Chen, H., Hou, J., Zhang, S., Liang, Y., Yang, G. & Yang, Y. Polymer solar cells with enhanced open-circuit voltage and efficiency. *Nat. Photon.* **3**, 649–653 (2009).
5 Zhou, H., Yang, L., Stuart, A. C., Price, S. C., Liu, S. & You, W. Devleopment of fluorinated benzothiadiazole as a structural unit for a polymer solar cell of 7% efficiency. *Angew. Chem. Int. Ed.* **123**, 3051–3054 (2011).
6 Yu, G., Gao, J., Hummelen, J. C., Wudl, F. A. & Heeger, A. J. Polymer photovoltaic cells: enhanced efficiencies via a network of internal donor-acceptor heterojunctions. *Science* **270**, 1789–1791 (1995).
7 Chang, W.-H., Gao, J., Dou, L., Chen, C.-C., Liu, Y. & Yang, Y. Side-chain tunability via triple component random copolymerization for better photovoltaic polymers. *Adv. Energy Mater.* **4**: 4 1300864 1-6 (2014).
8 Perepichka, I. F., Perepichka, D. F., Meng, H. & Wudl, F. Light-emitting polythiophenes. *Adv. Mater.* **17**, 2281 (2005).
9 Osaka, I. & McCullough, R. D. Advances in molecular design and synthesis of regioregular polythiophenes. *Acc. Chem. Res.* **41**, 1202–1214 (2008).

10 McCullough, R. D., Lowe, R. D., Jayaraman, M. & Anderson, D. L. Design, synthesis, and control of conducting polymer architectures: structurally homogeneous poly(3-alkylthiophenes). *J. Organ. Chem.* **58**, 904–912 (1993).
11 Koster, L. J. A., Mihailetchi, V. D. & Blom, P. W. M. Ultimate efficiency of polymer/fullerene bulk heterojunction solar cell. *Appl. Phys. Lett.* **88**, 093511 (2006).
12 Chen, T.-A., Wu, X. & Rieke, R. D. Regiocontrolled Synthesis of Poly(3-alkylthiophenes) Mediated by Rieke Zinc: Their Characterization and Solid-State Properties. *J. Am. Chem. Soc.* **117**, 233–244 (1995).
13 Saunders, B. R. & Turner, M. L. Nanoparticle-polymer photovoltaic cells. *Adv. Colloid Interface Sci.* **138**, 1–23 (2008).
14 Bundgaard, E. & Krebs, F. C. Low-band-gap conjugated polymers based on thiophene, benzothiadiazole, and benzobis(thiadiazole). *Macromolecules* **39**, 2823–2831 (2006).
15 Bundgaard, E. & Krebs, F. C. Low band gap polymers for organic photovoltaics. *Sol. Energy Mater. Sol. Cell* **91**, 954–985 (2007).
16 Geeta, S. & Josemon, J. Synthesis and characteriazation of 3,4-diaryl-substituted polythiophene derivatives. *Polym. Int.* **60**, 1010–1015 (2011).
17 Theander, M., Inganas, O., Mammo, W., Olinga, T., Svensson, M. & Andersson, M. R. *J. Phys. Chem. B* **103**, 7771–7780 (1999).
18 Johansson, T., Mammo, W., Svensson, M., Andersson, M. R. & Inganas, O. Electrochemical bandgaps of substituted polythiophenes. *J. Mater. Chem.* **13**, 1316–1323 (2003).
19 Peng, R., Yang, F., Ouyang, X., Liu, Y., Kim, Y. S. & Ge, Z. Enhanced photovoltaic performance of inverted polymer solar cells by tuning the structures of titanium dioxide. *Thin Solid Films* **545**, 424–428 (2013).
20 Munazza, S., Raja, S. A., Elisabeth, K. & Steffi, S. Synthesis and properties of novel low-band-gap thienopyrazine-based poly(heteroarylenevinylene)s. *Macromloecules* **39**, 7844–7853 (2006).
21 Kristof, C., Sofie, F., Thomas, J. C., Laurence, L., Jan, G. & Dirk, V. Low band gap donor-acceptor conjugated polymers toward organic solar cells applications. *Macromolecules* **40**, 65–72 (2007).
22 De Lceuw, D. M., Simenon, M. M. J., Brown, A. R. & Einerhand, R. E. F. Stability of n-type doped conducting polymers and consequences for polymeric microelectronic devices. *Synth. Met.* **87**, 53–59 (1997).
23 Janietz, S., Bradley, D. D. C., Grell, M., Giebeler, C., Inbasekaran, M. & Woo, E. P. Electrochemical determination of the ionization potential and electron affinity of poly (9,9-doctylfluorene). *Appl. Phys. Lett.* **73**, 2453 (1998).
24 Chen, Z.-K., Huang, W., Wang, L.-H., Kang, E.-T., Chen, B. J., Lee, C. S. & Lee, S. T. A family of electroluminescent silyl-substituted poly(p-phenylenevinylene)s: synthesis, characterization, and structure-property relationships. *Macromolecules* **33**, 9015–9025 (2000).
25 Chen, Y., Chang, C., Cheng, Y. & Hsu, C. Synthesis of a new ladder-type benzodi(cyclopentadithiophene) arene with forced planarization leading t o an enhanced efficiency of organic photovoltaics. *Chem. Mater.* **24**, 3964–3971 (2012).
26 Zhang, M., Guo, X. & Li, Y. Photovoltaic performance improvement of D–A copolymers containing bithiazole acceptor unit by using bithiophene bridges. *Macromolecules* **44**, 8798–8804 (2011).
27 Zhou, H., Zhang, Y., Seifter, J., Collins, S. D., Luo, C., Bazan, G. C., Nguyen, T. Q. & Heeger, A. J. High-efficiency polymer solar cells enhanced by solvent treatment. *Adv. Mater.* **25**, 1646–1652 (2013).
28 Yang, M., Chen, X., Zou, Y., Pan, C., Liu, B. & Zhong, H. A solution-processable D–A–D small molecule based on isoindigo for organic solar cells. *J. Mater. Chem.* **48**, 1014–1020 (2013).
29 Zheng, Q., Jung, B., Sun, J. & Katz, H. E. Ladder-typer oligo-p-phenylene-containing copolymers with high open-circuit voltages and ambient photovoltaic activity. *J. Am. Chem. Soc.* **132**, 5394–5404 (2010).
30 Li, D., Qian, G. & Wang, Z. Synthesis and characterizations of conjugated copolymers containing benzo[f]isoindole-1,3-dione and diketopyrrolopyrrole units. *Polymer* **54**, 5543–5552 (2013).